Resonance Raman Study of Shell Morphology in InP/ZnSe/ZnS Core/Shell/Shell Nanocrystals

Paul Cavanaugh,[1] Ilan Jen-La Plante,[2] Christian Ippen,[2] Ruiqing Ma,[2] David F. Kelley,[1]* and Anne Myers Kelley[1]*

[1]Department of Chemistry and Biochemistry, University of California, Merced, 5200 North Lake Road, Merced, CA 95340

[2] Nanosys Inc., 233 S. Hillview Dr, Milpitas, CA 95035

*David F. Kelley: e-mail dfkelley@ucmerced.edu, tel. (209) 228-4354. Anne Myers Kelley: e-mail amkelley@ucmerced.edu, tel. (209) 228-4345.

Abstract

Resonance Raman spectra and absolute cross-sections of InP/ZnSe/ZnS core/shell/shell nanocrystals have been obtained at excitation wavelengths of 501.7, 457.9, and 410 nm. Eight different structures having nearly the same lowest excitonic absorption wavelength but significantly different stoichiometries are compared. The Raman spectra show phonon features attributable to both the InP core and the ZnSe shell. The largest differences among the structures are seen in the ZnSe phonon region using excitation at 457.9 nm, on the low-energy edge of the absorption features having significant contributions from the ZnSe shell. Here, structures that are nearly stoichiometric (In:P ratio ≈ 1.0) show a sharp, strongly polarized peak near the bulk ZnSe phonon frequency (~250 cm^{-1}) and a weak lower-frequency shoulder with a higher depolarization ratio. Structures having excess indium show a stronger low-frequency shoulder near 225 cm^{-1} and lower integrated Raman intensities throughout the ZnSe phonon region. These changes are attributed to the presence of indium atoms in the ZnSe shell. These results support a previous assignment of a slow rise component in the time-resolved photoluminescence spectra of nonstoichiometric structures to transient trapping of holes at indium defects in the shell.

Introduction

Indium phosphide nanocrystals are being actively studied as replacements for cadmium selenide in luminescent materials applications. Cadmium selenide quantum dots (QDs) have well-established synthetic protocols and their spectroscopy and photophysics have been studied extensively. By changing their structural and surface characteristics, they can be engineered to have long working lifetimes in practical devices. However, there are strong incentives to find alternative materials that do not contain toxic metals such as cadmium. Indium phosphide QDs have some highly desirable qualities including low toxicity and an emission wavelength that is readily tunable over a wide range because of the small effective mass of the electron. Recently reported synthetic methods produce samples with high monodispersity and accordingly narrow emission bandwidths, and high photoluminescence (PL) quantum yields.[1-6] While this is significant progress toward InP QDs as technologically viable materials, there remains much that is not known about the structure, spectroscopy, and photophysics of these materials.

A recent study examined in detail the time-resolved PL kinetics from a series of red-emitting InP/ZnSe/ZnS core/shell/shell QDs with high quantum yields.[7] Most samples exhibited nearly single exponential PL decay kinetics. However, many of the samples also exhibited a delayed rise of the PL, which was fit to a rise time of several hundred picoseconds and an amplitude of 0-12% of the total PL. A number of possible mechanisms were considered for this slow rise time, and the one most consistent with all of the experimental data was found to be reversible, transient trapping of holes at indium dopants in the ZnSe shell. This led us to explore resonance Raman spectroscopy as a way to directly probe the perturbations to the ZnSe shell phonons by indium defects.

Ref. 8 gives the ionization potentials of InP, ZnSe, and ZnS as 5.85, 6.82, and 7.5 eV, respectively, and the electron affinities as 4.51, 4.12, and 3.8 eV, respectively (Figure 1). The small

conduction band and large valence band offset make InP-ZnSe a quasi-type-II, much like CdSe-CdS. ZnS has band offsets that are type-I with respect to both InP and ZnSe. With the larger bandgap, the resonant excitonic transitions probed in this work have almost no contribution from the outer shell material (ZnS) and we see no ZnS phonons in our spectra, so we do not further discuss this material. The optical phonons of bulk InP and bulk ZnSe span the region from 300-350 and 200-260 cm^{-1}, respectively.[9-10] The Raman spectra of bulk InP are dominated by the longitudinal optical (LO) phonon at 349 cm^{-1} and the transverse optical (TO) phonon at 306 cm^{-1}.[11] Resonance Raman spectra of InP nanocrystals of widely varying sizes and qualities show peaks fairly close to these bulk frequencies, plus overtones of these modes.[12-14] The Raman spectra of bulk ZnSe show mainly the LO phonon at 253 cm^{-1},[15] with a much weaker TO phonon at 207 cm^{-1}. The resonance Raman spectra of pure ZnSe QDs show almost exclusively the LO phonon, shifted to slightly lower frequencies in smaller QDs, and its overtones.[16-17] InP/ZnSe core/shell QDs have also been examined by several groups.[14, 18-20] The resonance Raman spectra of these materials exhibit phonons similar to those of pure InP and pure ZnSe QDs, but the ZnSe LO phonon, in particular, tends to be shifted to lower frequencies and to have a shoulder between the bulk TO and LO frequencies whose shape and intensity vary greatly. These features, and their interpretation, are further discussed below.

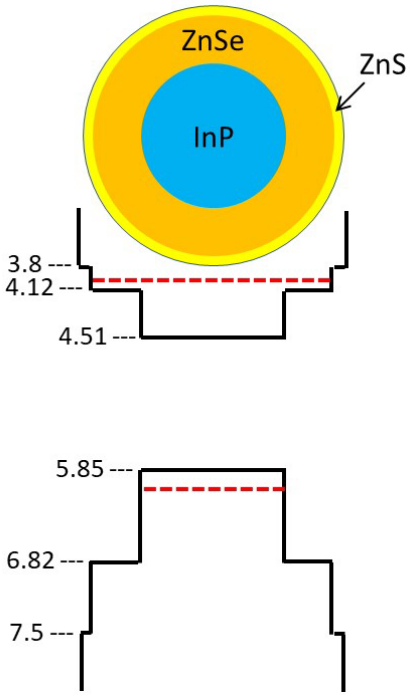

Figure 1. Energy level diagram of InP/ZnSe/ZnS core/shell/shell quantum dots. Red dashed lines show approximate energies of the quantum confined lowest electron and hole states.

Methods

Structures with a nominally spherical InP core, an intermediate ZnSe shell, and a thin outer shell of ZnS were synthesized and characterized as discussed in ref. 7. Resonance Raman spectra were obtained for eight structures that have their lowest excitonic peak maxima at 604-621 nm. Table 1 summarizes the longest-wavelength absorption maxima, core diameters and shell thicknesses, and stoichiometries of these structures. We note that the volume of ZnSe in these structures is 10-20 times greater than the InP volume. Samples are named by their In/P mole ratios, with their exciton wavelength-based names from ref. 7 also given. Figure 1 shows the absorption spectra dissolved in cyclohexane, the solvent employed for the resonance Raman measurements. This solvent was chosen because its Raman spectrum interferes minimally with that of the QDs.

Table 1. Characterization of samples studied

sample name (in ref. 7)	dimensions: InP diam/ ZnSe thick/ ZnS thick (nm)	slow rise fraction (ref. 7)	In/P atom ratio	atom fraction indium in shell
R0.99 (609 Red)	3.05/2.51/0.37	2.4%	0.99	0%
R1.04 (614 Red B)	3.12/2.51/0.34	0%	1.04	0.22%
R1.09 (621 Red)	3.16/1.80/0.08	10.2%	1.09	0.92%
R1.11 (614 Red A)	3.12/2.73/0.37	6.4%	1.11	0.51%
R1.48 (605 Red B)	2.90/1.82/0.03	11.4%	1.48	4.1%
R1.54 (608 Red)	2.90/1.68/0.05	8.2%	1.54	5.1%
R1.58 (604 Red)	3.04/2.01/0.30	6.6%	1.58	4.1%
R1.63 (605 Red A)	2.90/2.25/0.05	12.4%	1.63	3.6%

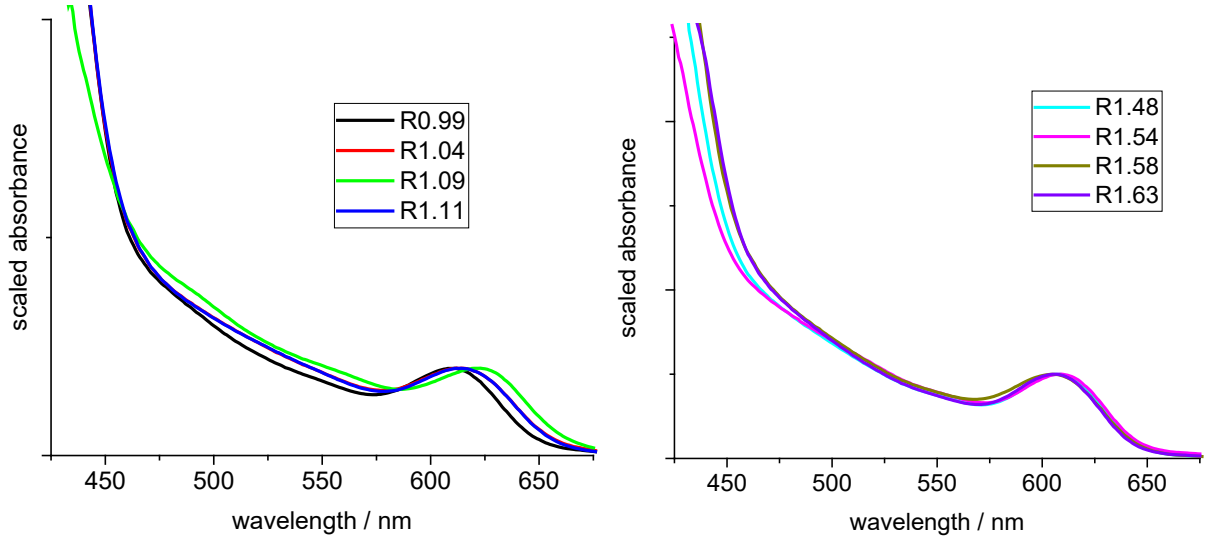

Figure 2. Optical absorption spectra of the eight samples studied, all scaled to the same absorbance maximum at the peak of the lowest exciton.

The Raman instrumentation and general methods were as described in ref. 21. The QDs were dissolved in cyclohexane at concentrations of 10-20 μM, giving an optical density at the lowest excitonic maximum of about 0.3-0.5/mm. The samples were contained in 1 mm fused silica cuvettes and the Raman scattering was collected in a backscattering geometry. In most experiments no polarization selection was employed. For the depolarization ratio measurements the polarization of the incident laser was rotated between horizontal and vertical while a fixed polarization of scattered light was detected, and the measured relative intensities of parallel and perpendicular scattering were corrected for instrument throughput using the known value of 0.75 for the depolarization ratio ($\rho = I_{perp}/I_{par}$) of the cyclohexane 424 cm^{-1} line.[22] Excitation at 501.7 nm and 457.9 nm was obtained from an argon-ion laser. Excitation at 410 nm was obtained from a frequency-doubled Ti:sapphire laser producing 1-2 ps pulses at 82 MHz. The wavenumber axes were calibrated using the 801 cm^{-1} cyclohexane line. The excitation beam was focused onto the

sample using a 10x microscope objective at an average power of about 0.75 mW, and typically signal was accumulated for 60 min on each sample.

The QDs studied all have PL quantum yields greater than 75% and are difficult to quantitatively quench because of the presence of the ZnSe and ZnS shells. Accordingly, no quenching was attempted and only excitation wavelengths that place the Raman scattering well to the blue of the strong PL were employed. The resulting Raman spectra have weak backgrounds from scattered laser light, the high-frequency tail of the PL, and broad Raman scattering from the fused silica cuvette. The latter is difficult to distinguish from Raman scattering from overtones, so no effort was made to quantitate overtone intensities in this work. A smooth curve was empirically fit to the background and subtracted from the displayed spectra. The Raman spectra in the 150-500 cm^{-1} range, as well as near the 801 cm^{-1} cyclohexane solvent peak, were then fit to a sum of Voigt profile peaks plus a baseline using OriginPro 2016 to obtain the positions and integrated intensities of each of the peaks. The intensities were corrected for reabsorption assuming a 180 degree backscattering geometry.

Absolute differential Raman cross-sections for the QDs were obtained by ratioing the integrated areas of the QD Raman peaks to those of the cyclohexane 801 cm^{-1} line as described in ref. 21 using the cyclohexane Raman cross-sections from ref. 23. The QD concentrations for the absolute cross-section calculations were obtained from molar absorptivities calculated as in ref. 16 and summarized in the Supporting Information.

Results

Figure 2 shows charge distributions for the $1S_e1S_h$, $1S_e2S_h$, and $1P_e1P_h$ excitonic states calculated from a simple effective-mass particle-in-a-sphere model using parameters given in the Supporting Information. The $1S_e2S_h$ and $1P_e1P_h$ states are calculated to be about 0.57 and 1.25 eV

above the $1S_e1S_h$, corresponding to about 477 and 378 nm, respectively. While these calculations are very approximate and do not include the excitonic transitions allowed in structures that deviate from spherical symmetry, they convey the basic idea that 501.7 nm excitation is on resonance with excitons localized mainly in the core and at the core/shell interface while 410 nm excitation is on resonance with excitons localized mainly in the shell region. These wavefunctions also suggest that the exciton produced by excitation at 457.9 nm will be largely confined to the core but have significant electron and to a lesser extent hole density in the inner part of the shell, near the core-shell interface.

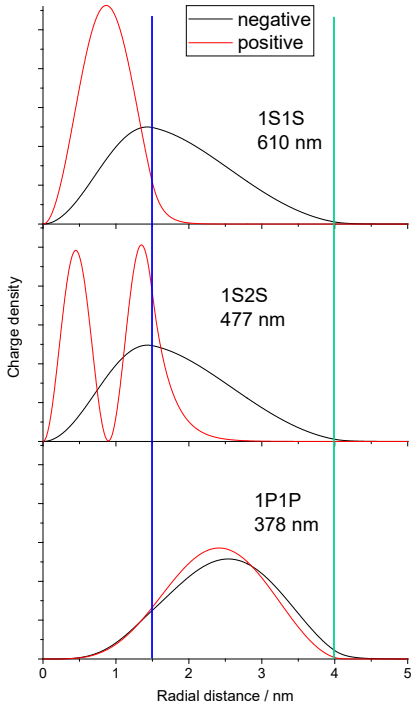

Figure 3. Calculated positive (hole) and negative (electron) charge densities calculated for the two lowest S-symmetry and one lowest P-symmetry excitons. The blue and green lines indicate the boundaries of the InP core (1.5 nm radius) and ZnSe shell (2.5 nm thick). See Supporting Information for further details.

Figures 4-6 show the resonance Raman spectra of the eight structures at three excitation wavelengths. All of the structures exhibit the same three sets of peaks in the 200-450 cm^{-1} region. A poorly resolved pair of peaks in the 215-250 cm^{-1} range is attributed to phonons of the ZnSe shell. Peaks near 323 and 352 cm^{-1}, plus an unresolved feature between these two peaks, arise from phonons of the InP core. Peaks near 383 and 424 cm^{-1} are weak Raman lines of the cyclohexane solvent. The ZnSe phonons are weak compared with the InP phonons at 501.7 nm because the excitons resonant with this wavelength are largely localized in the core. The ZnSe and InP phonons have comparable intensities with 457.9 nm excitation, which is resonant or near-resonant with a combination of excitons distributed over both core and shell. Finally, the InP peaks are almost invisible when excited at 410 nm, resonant with excitons that have a much larger contribution from the shell. As the volume of ZnSe is 10-20 times greater than the volume of InP in these structures, if the excitons were distributed equally between core and shell and the exciton-phonon coupling strengths were similar, the shell phonons would be overwhelmingly dominant.

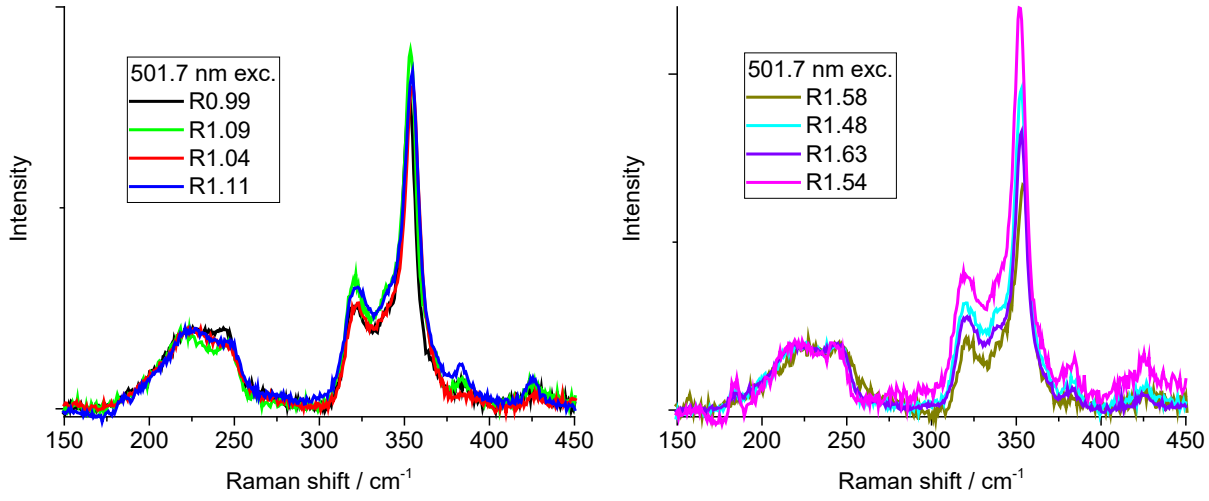

Figure 4. Resonance Raman spectra of the samples listed in Table 1 at 501.7 nm excitation. All spectra are background subtracted and scaled to the peak intensity in the 220-250 cm^{-1} region.

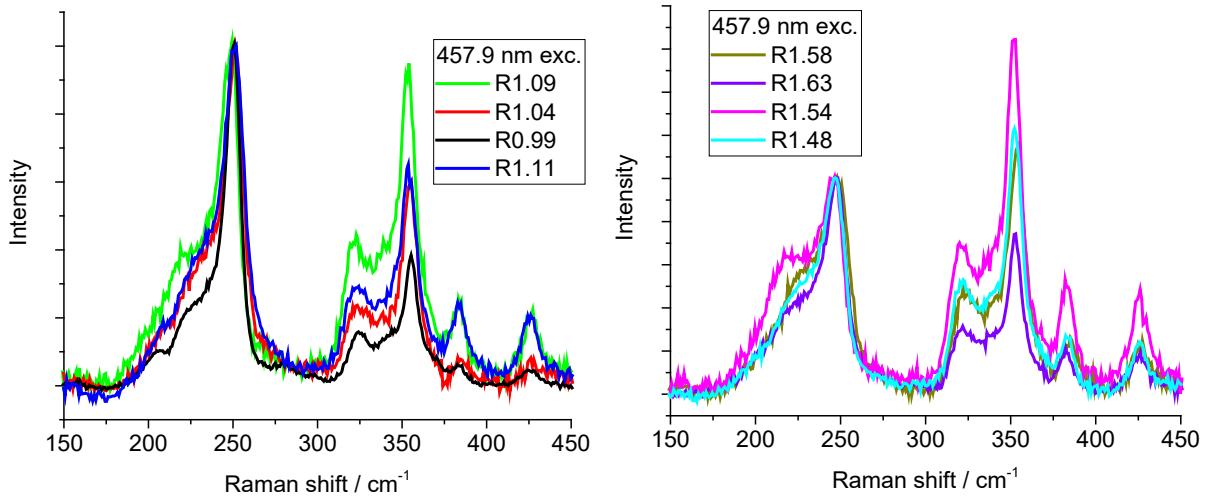

Figure 5. Resonance Raman spectra of the structures listed in Table 1 at 457.9 nm excitation. All spectra are background subtracted and scaled to the peak intensity in the 220-250 cm^{-1} region.

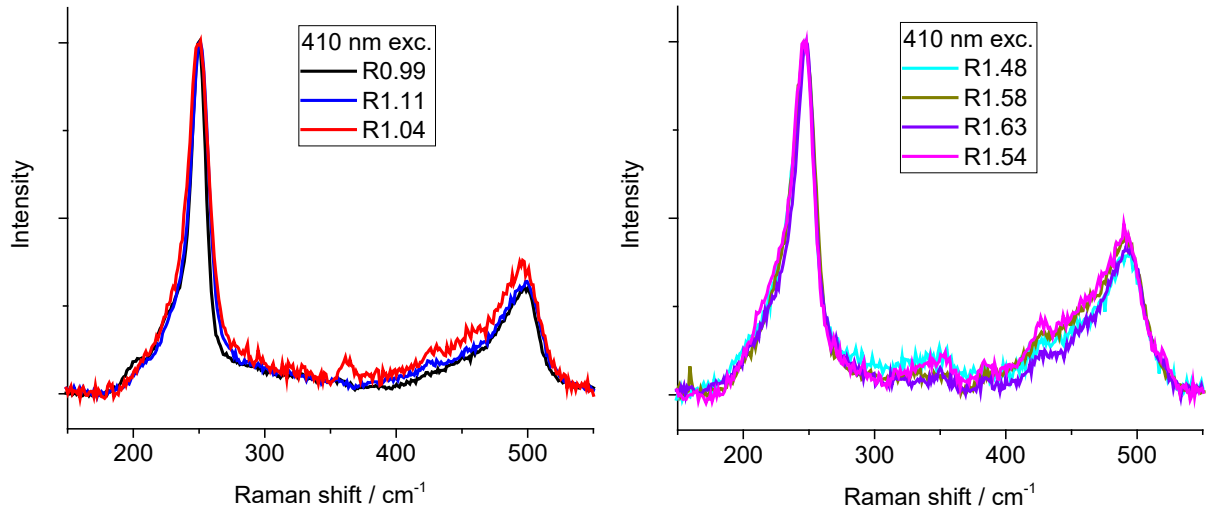

Figure 6. Resonance Raman spectra of seven of the structures listed in Table 1 at 410 nm excitation. All spectra are background subtracted and scaled to the peak intensity in the 220-250 cm^{-1} region.

The spectra of all eight structures at 501.7 nm excitation are fairly similar. There are small differences in the frequencies and relative intensities of both the ZnSe and InP peaks as well as in

the overall intensity of the InP features relative to the ZnSe features, but the differences are not striking. There is a small variation of the InP phonon frequencies that correlates roughly with shell thickness and is straightforward to rationalize. ZnSe has a smaller lattice parameter than InP (0.567 nm *vs*. 0.586 nm) so the InP core is subject to a radially compressive strain, raising the frequencies of its phonons.[20, 24] In contrast, the spectra of different structures at 457.9 nm excitation are very different, most notably in the intensity of the low-frequency ZnSe shoulder relative to the higher-frequency ZnSe peak, and also in the overall intensity of the features in the ZnSe region relative to those in the InP region. In some 457.9 nm excited spectra (*e.g*. R0.99) there are clearly two distinct components to the low-frequency shoulder. At 410 nm the spectra of the different structures are again generally similar, varying somewhat in the broadening to lower frequencies of the ZnSe peak.

Table 2. Peak fitting at 457.9 nm excitation, corrected for reabsorption. Estimated uncertainties are ±0.5 cm^{-1} for the peak frequencies, ±40% for the low frequency to high frequency intensity ratio, and ±20% for the differential Raman cross-section.

sample	ZnSe high freq /cm^{-1}	InP high freq /cm^{-1}	ZnSe low freq /high freq int ratio	$d\sigma_{ZnSe}/d\Omega$ / 10^{-7} Å^2	$[(d\sigma_{ZnSe}/d\Omega)$ /vol ZnSe] / 10^{-10} Å^2 nm^{-3}
R0.99	250.3	355.2	0.41	1.07	4.1
R1.04	250.9	354.7	0.60	0.70	2.6
R1.09	248.0	352.5	0.88	0.25	1.7
R1.11	250.4	353.4	0.72	0.52	1.6
R1.48	246.7	353.6	0.93	0.25	1.9
R1.54	245.5	351.7	1.71	0.20	1.6
R1.58	248.8	354.0	1.56	0.31	1.8
R1.63	247.3	352.5	0.48	0.47	2.4

Table 3. Peak fitting at 410 nm excitation. Estimated uncertainties are ±0.5 cm^{-1} for the peak frequencies and ±20% for the differential Raman cross-section.

sample	ZnSe high freq /cm^{-1}	$d\sigma_{ZnSe}/d\Omega$ / 10^{-7} Å^2	$[(d\sigma_{ZnSe}/d\Omega)$ /vol ZnSe] / 10^{-9} Å^2 nm^{-3}
R0.99	249.7	10.6	4.1
R1.04	250.0	12.0	4.5
R1.11	250.9	6.4	2.0
R1.48	248.2	2.8	2.1
R1.54	246.9	2.5	2.0
R1.58	248.0	2.6	1.5
R1.63	248.4	4.5	2.3

Tables 2 and 3 summarize some of the salient quantitative features of the 457.9 nm and 410 nm-excited spectra, obtained by fitting the background-subtracted spectra to a sum of peaks. The analogous table for 501.7 nm excitation is found in the Supporting Information. The InP region required three peaks to give good fits, while either two or three peaks were used in the ZnSe region. Table 2, for 457.9 nm excitation, gives the center frequencies of the highest-frequency ZnSe and InP peaks, the intensity ratio of the low-frequency shoulder (one or the sum of two peaks) to the high-frequency peak in the ZnSe region, the differential Raman cross-section for the sum of the ZnSe peaks, and the cross-section normalized to the volume of the ZnSe shell. Table 3, for 410 nm excitation, gives the center frequency of the ZnSe peak and its differential cross-section with and without shell volume scaling. The entries on the first two lines, R0.99 and R1.04, are the most nearly stoichiometric (smallest amount of excess indium, see Table 1) and also show the smallest contribution of the slowly rising component to the time-resolved emission spectra in ref. 7. These two samples have the highest frequency for each of the Raman lines (together with

R1.11), the lowest low-frequency to high-frequency ZnSe intensity ratio (together with R1.63), and the strongest ZnSe Raman scattering at both 457.9 and 410 nm excitation.

The polarization of the Raman scattering was examined for three samples (R0.99, R1.54, and R1.58) and representative results at 457.9 nm excitation are shown in Figure 7. It is clear that the higher-frequency component of the ZnSe band is much more strongly polarized than the lower-frequency component for structure R0.99, while the two components appear to be similarly polarized for structure R1.58. We note that the cyclohexane peak at 384 cm^{-1} is almost totally polarized (almost no intensity in the perpendicular spectrum) as has been previous reported, while the 424 cm^{-1} line should have a depolarization ratio of 0.75.[22] The spectra in Figure 7 have not been corrected for the wavelength-dependent polarization sensitivity of the spectrograph throughput, which would correct the raw depolarization ratios by relatively small factors of 0.9 to 1.3.

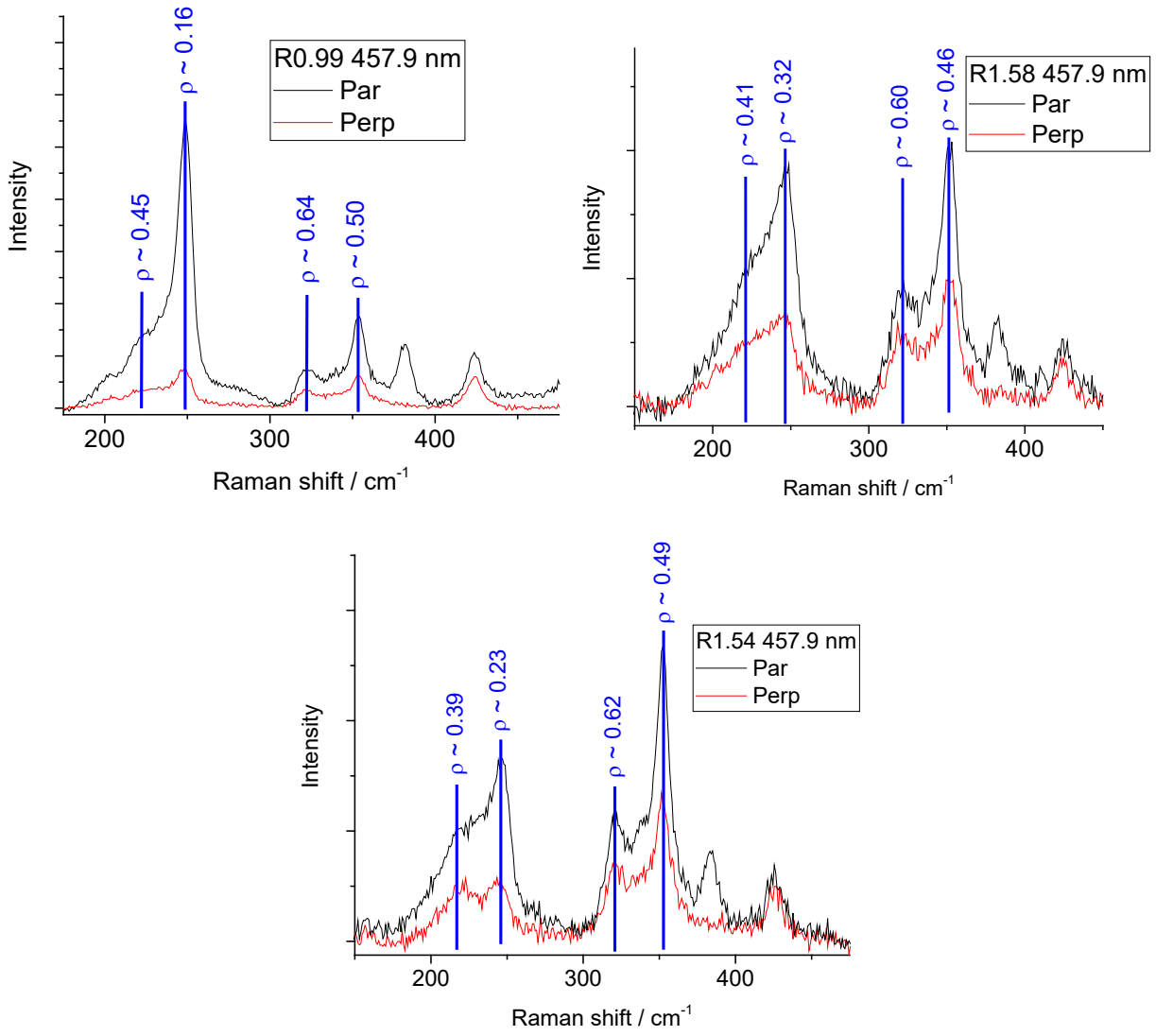

Figure 7. Resonance Raman spectra of three of the structures from Table 1 excited at 457.9 nm, with scattering polarized parallel (black) and perpendicular (red) to the laser polarization.

Discussion

The nanocrystals studied in this work are nominally InP/ZnSe/ZnS core/shell/shell quantum dots having an approximately spherical geometry. However, elemental analysis shows that in most of these structures the In:P atomic ratio is considerably greater than unity (Table 1). Slightly different methods of synthesis and purification produce structures with variable

amounts of "excess" indium. The most likely location of the excess indium atoms is that they are substituting for zinc atoms either within the shell or at the InP/ZnSe core/shell interface. The "atom fraction indium in shell" column in Table 1 is obtained by assuming that the core is stoichiometric InP and that all of the excess indium atoms substitute for zinc atoms in the ZnSe shell. Previous studies of InP/ZnSe photophysics have also identified indium impurities in the ZnSe shell and have associated these with nonradiative recombination centers that decrease the photoluminescence quantum yields.[6, 25-26] In contrast, our recent PL studies[7] showed that at the concentration of indium impurities in the shell of the present QDs, these indium dopants produce rapid and reversible hole trapping that slightly delays the luminescence but has no clear effect on the quantum yield.

Basic principles can be used to make some reasonable estimates for the effect of Zn→In substitution on the vibrational frequencies and hence the Raman spectra of ZnSe. Other things being equal, the vibrational frequency is proportional to the inverse square root of the reduced mass of the vibration. The LO phonon in CdSe appears near 210 cm^{-1} compared with ZnSe near 250 cm^{-1}, and indium has nearly the same atomic mass as cadmium. Thus, a reasonable first guess for the frequency of an LO phonon in "InSe" would be around 210 cm^{-1}. Since only a small fraction of the zinc atoms are replaced by indium the frequency should not be this low, and the interatomic force field is surely different than in CdSe, but we do expect indium defects in the ZnSe shell to lower the frequency of the ZnSe phonons. This is consistent with the observations in Table 2 that the structures with more excess indium have a slightly lower frequency for the main ZnSe peak as well as greater relative intensity in the low-frequency shoulder. Similar frequency phonons would also be expected at the InP-ZnSe interface, where direct In-Se bonding can occur.

Dependence of the Raman spectra on excitation wavelength

Comparing the spectra of any given structure at 410, 457.9, and 501.7 nm, there are two obvious trends. First, the intensities of the ZnSe modes decrease relative to those of the InP modes as the excitation is tuned to longer wavelengths. This is a straightforward consequence of the lower-energy resonant excitons being more localized to the InP core. Second, the lower-frequency component of the ZnSe feature becomes relatively stronger and the higher-frequency component shifts 2-6 cm^{-1} to lower frequencies as the excitation is tuned from 457.9 nm to 501.7 nm. This strongly suggests that the lower-frequency component is dominated by motions of ZnSe groups at or very near the interface with the InP core, as the lowest-energy excitons extend only slightly into the shell. A similar effect was observed in CdSe/CdS core/shell QDs studied previously.[27] There, the peak frequency of the CdS "LO" phonon dropped from 301 cm^{-1} to 285-290 cm^{-1} as the excitation wavelength was tuned from 5000 cm^{-1} above the lowest, core-localized excitonic transition to resonance with that lowest exciton, indicating that the CdS modes at the interface with the CdSe core are lower in frequency than the CdS modes in the bulk shell. This interpretation is further supported by the spectra of InP/ZnSe core/shell QDs with varying shell thicknesses. Ref. 20 shows that at a fixed excitation wavelength (514 nm, obtained using a silicon substrate to quench the photoluminescence), the intensity of the higher-frequency ZnSe component increases relative to that of the lower-frequency component and both components shift to slightly higher frequencies as the shell thickness is increased from 2 to 13 monolayers. The structures studied in this work have relatively thick ZnSe shells of 6-10 monolayers.

Between 501.7 and 457.9 nm excitation the ZnSe modes gain intensity relative to the InP modes, the high-frequency ZnSe component gains intensity relative to the low-frequency component, and the high-frequency component moves to higher frequency by 2-6 cm^{-1} (see Tables 2 and S1). The low-frequency component also appears to move to higher frequency, but its

frequency is more difficult to determine accurately. As the Raman shift of a given vibrational mode is independent of excitation wavelength, these frequency shifts indicate that different sets of normal modes are resonance enhanced at the two different excitation wavelengths. By analogy with previous calculations on CdSe QDs,[28] the "ZnSe LO phonon" in QDs of this size should consist of dozens of different normal modes that involve similar atomic motions at the unit cell level but differ in their nodal patterns and/or spatial distributions across the ZnSe shell, and have slightly different frequencies. At 457.9 nm excitation the high-frequency ZnSe component is more strongly polarized than the low-frequency component, particularly for structure 609; we find ρ = 0.1-0.2 for the high-frequency component and ρ = 0.4-0.5 for the low-frequency component. This shows that the two components are resonance enhanced from different sets of excitonic transitions, consistent with their having different spatial distributions—presumably largely interface-localized for the low-frequency component and distributed throughout the shell for the high-frequency component.

At 410 nm excitation there appears to be a single peak in the ZnSe region, roughly corresponding to the high-frequency component. The lower-frequency component is not resolved but contributes to broadening the main peak, and this broadening is most pronounced in those structures that have stronger low-frequency components at 457.9 nm. These observations are consistent with the resonance enhancement at this wavelength involving excitons distributed throughout the shell, as indicated in the wavefunction calculations in Figure 3. Comparison with the spectra obtained with longer wavelength excitation indicates that some, but not all, of the intensity in the low-frequency shoulder is associated with the InP-ZnSe interface.

Dependence of the resonance Raman spectra on stoichiometry

At 501.7 nm, where only the vibrations in the core and at the core/shell interface are being probed, all structures show similar spectra consistent with both ZnSe peaks arising largely from

phonons localized near the interface with the InP core. The spectra are not much affected by the presence or absence of excess indium in the shell. At 457.9 nm excitation, where the resonant excitons presumably extend further into the shell, the nonstoichiometric samples have more relative intensity in the lower-frequency ZnSe component. This suggests that substitution of indium atoms for zinc atoms in the shell causes some of the ZnSe phonons to shift down in frequency from the ~250 cm^{-1} characteristic of pure ZnSe to the 215-235 cm^{-1} range, overlapping the interface phonons present in all structures. Thus, stoichiometric structures such as R0.99 and R1.04 show primarily the unperturbed high-frequency component, while nonstoichiometric structures such as R1.58 and R1.54 have relatively more intensity in the low-frequency component.

Structures containing excess indium clearly show greater relative intensity in the low-frequency component of the ZnSe doublet at the shorter excitation wavelengths. This could result from a shift of the phonon frequencies to lower values because of the substitution of indium for zinc, and/or a change in the relative Raman enhancements of the lower-frequency *vs*. higher-frequency phonons. Clearly resonance enhancement plays some role, as the relative intensities of the two components of the ZnSe doublet vary much less at 501.7 nm excitation (Figure 4) than at 457.9 nm (Figure 5). The high-frequency component undergoes greater enhancement at 457.9 nm in the structures that contain little excess indium in the shell. This could be caused by differences in the spatial distribution of the excitonic wavefunctions in the presence of excess indium, indium-induced shifts of some of the resonance enhanced phonons to lower frequencies, and/or changes in the mode character of the phonons due to the excess indium. At present we cannot distinguish among these mechanisms.

Resonance Raman depolarization ratios

The Raman depolarization ratios exhibit significant differences among Raman lines and among structures that are not straightforward to interpret. As a point of reference, the Raman depolarization ratio for resonance with a single, nondegenerate electronic transition is $\rho = 1/3$ and the depolarization ratio for a perfectly isotropic structure (all electronic transitions degenerate along x, y, and z) is $\rho = 0$.[21, 29] While a perfect zincblende crystal is optically isotropic, any symmetry breaking caused by either the overall shape of the nanocrystal or the presence of defects will split the degeneracies of the states and result in nonzero depolarization ratios whose values depend strongly on the magnitude of the splitting. Experimental resonance Raman depolarization ratios for the LO phonon fundamentals in pure QDs vary from 0.1 to 0.4 in CdSe[21, 29-31] and 0.17 to 0.21 in ZnSe.[16] However, the depolarization ratios are strongly dependent on the interferences among excitonic transitions polarized in different directions that are coupled to the same phonons, and a simple model can produce depolarization ratios throughout the range from 0 to near 0.75 as shown in the Supporting Information. For the three structures examined (R0.99, R1.58, and R1.54), the measured depolarization ratios for the InP lines and for the lower-frequency ZnSe peak are all in the range from 0.39 – 0.64 with 457.9 nm excitation. Not surprisingly, the InP depolarization ratios are nearly independent of excess indium. We find that only the higher-frequency ZnSe peak of structure R0.99 has a depolarization ratio ($\rho \approx 0.16$) close to that previously measured for pure ZnSe QDs. This supports the assignment of the high-frequency ZnSe line in stoichiometric structures to Raman scattering from ZnSe in a nearly unperturbed environment, while the lower-frequency band involves resonance with excitons perturbed by the interface with the InP core and/or indium impurities in the shell.

Resonance Raman fundamental and overtone intensities

Another major difference between the stoichiometric structures and those with excess indium is that the stoichiometric structures show higher absolute scattering cross-sections for the Raman bands in the ZnSe region when excited at 457.9 nm and even more dramatically with excitation at 410 nm (Tables 2 and 3). This difference is most pronounced with 410 nm excitation when the cross-section is normalized to the ZnSe shell volume, *i.e.* the cross-section per ZnSe unit. Resonance Raman cross-sections depend on a complex set of factors that are difficult to quantitate in these systems: the transition dipole strengths of the resonant transitions, the extent of interference (constructive or destructive) among the contributing resonant transitions, the strength of exciton-phonon coupling, and the electronic dephasing rates.[21, 32] Interpretation of these intensity differences must await a better understanding of the identities and energies of the higher-energy excitonic transitions in these structures.

The overtone to fundamental (two-quantum to one-quantum) intensity ratios are often taken to be diagnostic of the strength of exciton-phonon coupling in semiconductor nanocrystals, although interference effects, dephasing rates, and detuning from resonance also influence overtone intensities.[33] The overtones appear to be very weak with 501.7 nm excitation and slightly stronger with 457.9 nm excitation, but they are difficult to distinguish from the broad background scattering from the fused silica windows in the 300-600 cm^{-1} range. At 410 nm excitation, however, the ZnSe overtones are very strong, roughly equal in integrated intensity to the fundamentals and fairly independent of the amount of excess indium (Figure 6). While pure ZnSe QDs excited at similar wavelengths show weaker overtones,[16] the 386-425 nm excitation employed in those studies was close to the lowest excitonic transition of the pure QDs while 410 nm excitation in the present core/shell/shell structures is resonant with multiple higher-energy

excitonic transitions. The reasons for the apparently stronger exciton-phonon coupling in the 410 nm excited spectra remain to be explored.

Conclusions

The presence of excess indium (In:P ratio > 1) in InP/ZnSe/ZnS core/shell/shell QDs manifests itself in the resonance Raman spectra in two principal ways. The relative intensity of the low-frequency component of the ZnSe doublet is increased when excited at the low-energy edge of the absorbance attributed mostly to ZnSe, and the overall intensity of the ZnSe Raman scattering is reduced when excited at 457.9 or particularly at 410 nm. Nearly stoichiometric structures (In:P ratio near unity) exhibit a resonance Raman spectrum in the region of the ZnSe phonons closely resembling that of pure ZnSe QDs in its frequency, band shape, and depolarization ratio.

Supporting Information

The Supporting Information is available free of charge at https://pubs.acs.org. Details of the wavefunction calculations in Figure 3, peak fitting results at 501.7 nm, a more complete treatment of resonance Raman depolarization ratios, calculations of the QD molar absorptivities, and sample Raman spectra prior to background subtraction.

Acknowledgments

This work was supported by NSF grant CHE-1506803 and by the U.S. Department of Energy's Office of Energy Efficiency and Renewable Energy (EERE) under the award number DEEE0009164. The views expressed herein do not necessarily represent the views of the U.S. Department of Energy or the United States Government.

References

1. Kim, Y.; Ham, S.; Jang, H.; Min, J. H.; Chung, H.; Lee, J.; Kim, D.; Jang, E., Bright and Uniform Green Light Emitting InP/ZnSe/ZnS Quantum Dots for Wide Color Gamut Displays. *ACS Appl. Nano Mater.* **2019**, *2*, 1496-1504.

2. Won, Y.-H.; Cho, O.; Kim, T.; Chung, D.-Y.; Kim, T.; Chung, H.; Jang, H.; Lee, J.; Kim, D.; Jang, E., Highly Efficient and Stable InP/ZnSe/ZnS Quantum Dot Light-Emitting Diodes. *Nature* **2019**, *575*, 634-641.

3. Jo, J.-H.; Jo, D.-Y.; Lee, S.-H.; Yoon, S.-Y.; Lim, H.-B.; Lee, B.-J.; Do, Y. R.; Yang, H., InP-Based Quantum Dots Having an InP Core, Composition-Gradient ZnSeS Inner Shell, and ZnS Outer Shell with Sharp, Bright Emissivity, and Blue Absorptivity for Display Devices. *ACS Appl. Nano Mater.* **2020**, *3*, 1972-1980.

4. Liu, P.; Lou, Y.; Ding, S.; Zhang, W.; Wu, Z.; Yang, H.; Xu, B.; Wang, K.; Sun, X. W., Green InP/ZnSeS/ZnS Core Multi-Shelled Quantum Dots Synthesized with Aminophosphine for Effective Display Applications. *Adv. Funct. Mater.* **2021**, 2008453.

5. Hahm, D.; Chang, J. H.; Jeong, B. G.; Park, P.; Kim, J.; Lee, S.; Choi, J.; Kim, W. D.; Rhee, S.; Lim, J.; Lee, D. C.; Lee, C.; Char, K.; Bae, W. K., Design Principle for Bright, Robust, and Color-Pure InP/$ZnSe_xS_{1-x}$/ZnS Heterostructures. *Chem. Mater.* **2019**, *31*, 3476-3484.

6. Li, Y.; Hou, X.; Dai, X.; Yao, Z.; Lv, L.; Jin, Y.; Peng, X., Stoichiometry-Controlled InP-Based Quantum Dots: Synthesis, Photoluminescence, and Electroluminescence. *J. Am. Chem. Soc.* **2019**, *141*, 6448-6452.

7. Nguyen, A.; Jen-La Plante, I.; Ippen, C.; Ma, R.; Kelley, D., Extremely Slow Trap-Mediated Hole Relaxation in Room Temperature InP/ZnSe/ZnS Quantum Dots. *J. Phys. Chem. C* **2021**, *125*, 4110-4118.

8. Stevanovic, V.; Lany, S.; Ginley, D. S.; Tumasb, W.; Zunger, A., Assessing capability of Semiconductors to Split Water Using Ionization Potentials and Electron Affinities Only. *Phys. Chem. Chem. Phys.* **2014**, *16*, 3706-3713.

9. Borcherds, P. H.; Alfrey, G. F.; Saunderson, D. H.; Woods, A. D. B., Phonon Dispersion Curves in Indium Phosphide. *J. Phys. C* **1975**, *8*, 2022-2030.

10. Hennion, B.; Moussa, F.; Pepy, G.; Kunc, K., Normal Modes of Vibration in ZnSe. *Phys. Lett.* **1971**, *36A*, 376-378.

11. Bedel, E.; Landa, G.; Carles, R.; Redoulks, J. P.; Renucci, J. B., Raman Investigation of the InP Lattice Dynamics. *J. Phys. C* **1986**, *19*, 1471-1479.

12. Guzelian, A. A.; Katari, J. E. B.; Kadavanich, A. V.; Banin, U.; Hamad, K.; Juban, E.; Alivisatos, A. P.; Wolters, R. H.; Arnold, C. C.; Heath, J. R., Synthesis of Size-Selected, Surface-Passivated InP Nanocrystals. *J. Phys. Chem.* **1996**, *100*, 7212-7219.

13. Seong, M. J.; Micic, O. I.; Nozik, A. J.; Mascarenhas, A.; Cheong, H. M., Size-Dependent Raman Study of InP Quantum Dots. *Appl. Phys. Lett.* **2003**, *82*, 185-187.

14. Manciu, F. S.; Tallman, R. E.; McCombe, B. D.; Weinstein, B. A.; Lucey, D. W.; Sahoo, Y.; Prasad, P. N., Infrared and Raman Spectroscopies of InP/II–VI Core-Shell Nanoparticles. *Physica E* **2005**, *26*, 14-18.

15. Taylor, W., The Raman Spectra of Cubic Zinc Selenide and Telluride. *Phys. Lett.* **1967**, *24A*, 556-558.

16. Gong, K.; Kelley, D. F.; Kelley, A. M., Resonance Raman Spectroscopy and Electron-Phonon Coupling in Zinc Selenide Quantum Dots. *J. Phys. Chem. C* **2016**, *120*, 29533-29539.

17. Kumar, P.; Singh, J.; Pandey, M. K.; Jeyanthi, C. E.; Siddheswaran, R.; Paulraj, M.; Hui, K. N.; Hui, K. S., Synthesis, Structural, Optical and Raman Studies of Pure and Lanthanum Doped ZnSe Nanoparticles. *Mat. Res. Bull.* **2013**, *49*, 144-150.

18. Brodu, A.; Ballottin, M. V.; Buhot, J.; van Harten, E. J.; Dupont, D.; La Porta, A.; Prins, P. T.; Tessier, M. D.; Versteegh, M. A. M.; Zwiller, V.; Bals, S.; Hens, Z.; Rabouw, F. T.; Christianen, P. C. M.; de Mello Donega, C.; Vanmaekelbergh, D., Exciton Fine Structure and Lattice Dynamics in InP/ZnSe Core/Shell Quantum Dots. *ACS Photonics* **2018**, *5*, 3353-3362.

19. Brodu, A.; Ballottin, M. V.; Buhot, J.; Dupont, D.; Tessier, M.; Hens, Z.; Rabouw, F. T.; Christianen, P. C. M.; de Mello Donega, C.; Vanmaekelbergh, D., Exciton-Phonon Coupling in InP Quantum Dots with ZnS and (Zn, Cd) Se Shells. *Phys. Rev. B* **2020**, *101*, 125413.

20. Rafipoor, M.; Tornatzky, H.; Dupont, D.; Maultzsch, J.; Tessier, M. D.; Hens, Z.; Lange, H., Strain in InP/ZnSe, S Core/Shell Quantum Dots from Lattice Mismatch and Shell Thickness—Material Stiffness Influence. *J. Chem. Phys.* **2019**, *151*, 154704.

21. Baker, J. A.; Kelley, D. F.; Kelley, A. M., Resonance Raman and Photoluminescence Excitation Profiles and Excited-State Dynamics in CdSe Nanocrystals. *J. Chem. Phys.* **2013**, *139*, 024702.

22. Durig, J. R.; Zheng, C.; Defrawy, A. M. E.; Ward, R. M.; Gounev, T. K.; Ravindranath, K.; Rao, N. R., On the Relative Intensities of the Raman Active Fundamentals, r_0 Structural Parameters, and Pathway of Chair–Boat Interconversion of Cyclohexane and Cyclohexane-d_{12}. *J. Raman Spectrosc.* **2009**, *40*, 197–204.

23. Trulson, M. O.; Mathies, R. A., Raman Cross Section Measurements in the Visible and Ultraviolet Using an Integrating Cavity: Application to Benzene, Cyclohexane, and Cacodylate. *J. Chem. Phys.* **1986**, *84*, 2068-2074.

24. Lange, H.; Kelley, D. F., Spectroscopic Effects of Lattice Strain in InP/ZnSe and InP/ZnS Nanocrystals. *J. Phys. Chem. C* **2020**, *124*, 22839-22844.

25. Freymeyer, N. J.; Click, S. M.; Reid, K. R.; Chisholm, M. F.; Bradsher, C. E.; McBride, J. R.; Rosenthal, S. J., Effect of Indium Alloying on the Charge Carrier Dynamics of Thick-Shell InP/ZnSe Quantum Dots. *J. Chem. Phys.* **2020**, *152*, 161104.

26. Reid, K. R.; McBride, J. R.; Freymeyer, N. J.; Thal, L. B.; Rosenthal, S. J., Chemical Structure, Ensemble and Single-Particle Spectroscopy of Thick-Shell InP−ZnSe Quantum Dots. *Nano Lett.* **2018**, *18*, 709-716.

27. Lin, C.; Gong, K.; Kelley, D. F.; Kelley, A. M., Electron-Phonon Coupling in CdSe/CdS Core-Shell Quantum Dots. *ACS Nano* **2015**, *9*, 8131-8141.

28. Kelley, A. M., Comparison of Three Empirical Force Fields for Phonon Calculations in CdSe Quantum Dots. *J. Chem. Phys.* **2016**, *144*, 214702.

29. Shiang, J. J.; Kadavanich, A. V.; Grubbs, R. K.; Alivisatos, A. P., Symmetry of Annealed Wurtzite CdSe Nanocrystals: Assignment to the C_{3v} Point Group. *J. Phys. Chem.* **1995**, *99*, 17417-17422.

30. Lin, C.; Gong, K.; Kelley, D. F.; Kelley, A. M., Size Dependent Exciton-Phonon Coupling in CdSe Nanocrystals Through Resonance Raman Excitation Profile Analysis. *J. Phys. Chem. C* **2015**, *119*, 7491-7498.

31. Shiang, J. J.; Craig, I. M.; Alivisatos, A. P., Resonance Raman Depolarization in CdSe Nanocrystals. *Z. Phys. D* **1993**, *26*, 358-360.

32. Myers, A. B., Excited Electronic State Properties from Ground-State Resonance Raman Intensities. In *Laser Techniques in Chemistry*, Myers, A. B.; Rizzo, T. R., Eds. Wiley: New York, 1995; pp 325-384.

33. Kelley, A. M., Resonance Raman Overtone Intensities and Electron-Phonon Coupling Strengths in Semiconductor Nanocrystals. *J. Phys. Chem. A* **2013**, *117*, 6143-6149.

TOC graphic